agriculture

MDPI

Article

A Method for Measuring Plant Spacing of Maize Seedlings Based on Improved YOLOv8

Peijing Zhang [1], Shixiong Yang [2] and Guifa Teng [2,3,*]

[1] School of Automation, Central South University, Changsha 410083, China; 8207230314@csu.edu.cn
[2] College of Information Science and Technology, Hebei Agricultural University, Baoding 071000, China; 13933293209@163.com
[3] School of Cyberspace Security, Hebei University of Engineering Science, Shijiazhuang 050091, China
* Correspondence: tguifa@hebau.edu.cn; Tel.: +86-0312-7521807

Abstract

The uniformity of maize plant spacing serves as a critical indicator for assessing sowing quality, seed vigor, and field seedling emergence stability. However, manual measurement is inefficient, and complex field conditions make automatic seedling detection and plant spacing measurement challenging. Aiming at the challenges of missed detection, insufficient accuracy for small targets, and large errors in plant spacing calculation under complex field conditions, this study constructs a high-quality dataset containing 693 maize seedling images and implements preprocessing enhancement for images degraded by haze or dust. An intelligent maize seedling detection and plant spacing measurement method based on improved YOLOv8 is proposed. The Global Attention Mechanism (GAM) is embedded into the backbone network to strengthen cross-dimension information interaction between channels and spaces, suppress background interference, and reduce the missed detection rate. The Bi-directional Feature Pyramid Network (BiFPN) is adopted to replace the original PAFPN for enhanced multi-scale feature fusion and deep semantic representation. A new 160 × 160 high-resolution small-object detection layer is added to significantly improve the detection performance of weak and small seedlings. Experimental results demonstrate that the improved model achieves a precision, recall, mAP50, and mAP50-95 of 89.4%, 90.3%, 94.4%, and 49.4%, respectively, which are 2.6, 0.5, 1.5, and 2.7 percentage points higher than those of the original YOLOv8 model. These results indicate that the proposed model improved maize seedling detection performance under complex field conditions. Automatic plant spacing calculation is realized based on detection outputs; the average plant spacing of the dataset is 30.42 cm, with a relative error of only 4.93% compared with the preset sowing spacing of 32 cm. The proposed method can efficiently accomplish field seedling identification, plant spacing quantification, and sowing quality evaluation, providing reliable technical support for precision maize sowing, seeder parameter optimization, and intelligent field management, which is of great significance for promoting the intelligent upgrading of grain crop production.

Keywords: maize seedlings; plant spacing measurement; YOLOv8; Global Attention Mechanism (GAM); Bi-directional Feature Pyramid Network (BiFPN); small-object detection; smart farm

Academic Editor: Marcus Randall

Received: 1 July 2026
Revised: 13 August 2026
Accepted: 13 August 2026
Published: 14 August 2026

1. Introduction

Maize is the largest grain crop in China and plays a strategic role in ensuring national food security and supporting the supply of raw materials for animal husbandry and industry. The formation of maize yield is highly dependent on sowing quality and field population structure. In particular, the uniformity of seedling spacing directly determines the utilization efficiency of light, water, and nutrients, thereby affecting emergence rate, stress resistance, and final yield [1–4]. Specifically, excessively dense spacing can intensify competition among seedlings for light, water, and nutrients, while overly sparse spacing may reduce canopy coverage and field resource utilization efficiency. Therefore, accurate plant spacing measurement is important for evaluating sowing quality and supporting subsequent field management. Traditional surveys of plant spacing and plant population rely mainly on manual measurement with rulers, mechanical counting, or contact-based sensor measurements. These methods suffer from low efficiency, strong subjectivity, potential damage to seedlings, and difficulty in conducting rapid large-scale field operations, making them inadequate for the demands of modern precision agriculture [5–7].

In recent years, UAV remote sensing and computer vision technologies have provided a transformative approach for non-contact, high-throughput field phenotyping [8,9]. In the field of object detection [10,11], the YOLO series has been widely applied to crop recognition, growth monitoring, and yield estimation due to its balance between speed and accuracy [12–14]. Nevertheless, the original YOLOv8 still has three main limitations: (1) the PAFPN feature fusion structure in the neck performs unweighted bidirectional feature transmission, resulting in insufficient utilization of multi-scale seedling features; (2) it lacks an efficient cross-dimensional attention mechanism, causing key targets to be easily overwhelmed by complex backgrounds and leading to missed detections; and (3) the resolution of the default detection layers is insufficient, resulting in relatively low localization accuracy for small and weak seedlings.

To address the above issues, this study proposes an improved YOLOv8-based method for maize seedling detection and plant spacing measurement. The main contributions are as follows: (1) a Global Attention Mechanism (GAM) is introduced to simultaneously enhance channel-wise and spatial feature interactions, reduce information loss, and improve the model's ability to focus on maize seedlings under complex backgrounds; (2) a weighted bidirectional feature pyramid network, namely BiFPN, is adopted to achieve adaptive multi-scale feature fusion, thereby strengthening both deep semantic information and shallow detailed representations; (3) a high-resolution 160 × 160 small-object detection head is added to specifically optimize the detection of small and weak maize seedlings, thereby reducing the missed detection rate; and (4) an end-to-end intelligent pipeline is constructed, covering image enhancement, seedling detection, plant spacing calculation, and sowing quality evaluation. The relative error is controlled within 4.93%, satisfying the practical requirements of field applications.

This study can provide efficient algorithmic support for the rapid evaluation of maize sowing quality, intelligent regulation of seeders, and precise identification of missing seedlings and broken ridges. It has important theoretical value and application prospects for improving the digitalization and precision of grain crop production.

2. Materials and Methods

2.1. Data Collection

The experimental site was located in a crop experimental field in Xinji City, Shijiazhuang, Hebei Province, China. The image data were collected in June 2025 during the maize seedling stage using UAVs and handheld devices, and a total of 833 original images were obtained. For UAV image acquisition, a DJI UAV equipped with an RGB camera was

https://doi.org/10.3390/agriculture16161746

used to collect nadir-view images, with the camera oriented vertically downward at a flight height of approximately 3 m above the ground. The original UAV images were stored in JPEG format with a resolution of 4000 × 3000 pixels. After quality screening, invalid images with blurring, overexposure, and severe occlusion were removed. Finally, a high-quality image dataset containing 693 images was constructed. The dataset covers different illumination conditions, weather conditions, planting densities, and field backgrounds, including bare soil, straw residues, ridge–furrow structures, and soil cracks, thereby improving the representativeness of the dataset under complex field conditions.

2.2. Preprocessing of Haze and Sand–Dust Images

In this study, approximately 80% of the images were collected under clear or normal atmospheric conditions, while about 20% were affected by natural haze or sand–dust conditions during field acquisition in June 2025 at the maize seedling stage. These images were included to better reflect variable field weather conditions in spring sowing areas and to evaluate the robustness of the proposed method. To address the problems of reduced image contrast and detail loss caused by haze and sand–dust conditions, degradation correction was performed based on the classical atmospheric scattering model:

$$I_X = J_X \times T_X + A(1 - T_X), \quad (1)$$

In the equation, I_X represents the observed image, J_X represents the ideal degradation-free image, T_X denotes the transmission map, and A refers to the global atmospheric light. To further enhance image details and improve the visibility of maize seedlings, the All-in-One Dehazing Network (AOD-Net), a CNN-based image dehazing model, was incorporated during the preprocessing stage [15]. AOD-Net reformulates the atmospheric scattering model and directly generates restored images from degraded inputs, which makes it suitable for improving the quality of field images before maize seedling detection. After preprocessing, the images showed more natural brightness, sharper edges, and more effective noise suppression, thereby improving the accuracy of subsequent seedling detection. Figure 1 presents a comparison of the preprocessing results for maize seedling images under haze and sand–dust conditions.

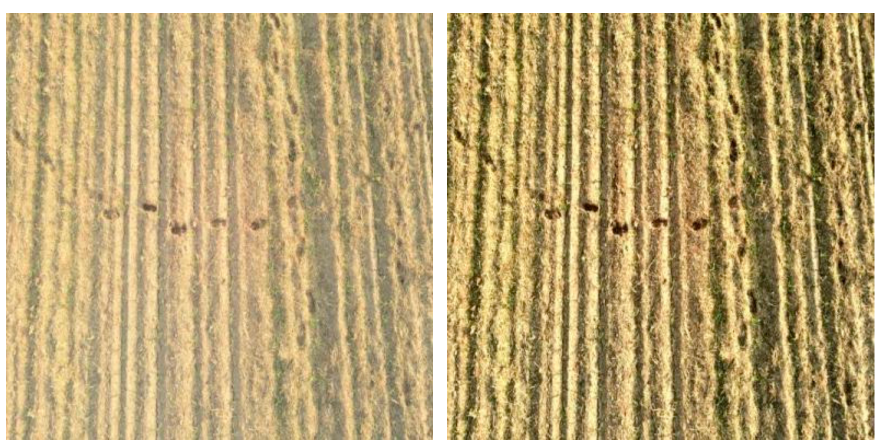

(**a**) (**b**)

Figure 1. Comparison of images before and after preprocessing. (**a**) Image before preprocessing. (**b**) Image after preprocessing.

2.3. Annotation and Dataset Partitioning

To achieve more efficient maize seedling recognition, the collected images were first manually annotated. LabelImg was used to annotate each maize seedling individually, with maize seedling defined as the only detection category. In total, 40,482 maize seedling

https://doi.org/10.3390/agriculture16161746

instances were annotated from the 693 images. After annotation, all labels were manually checked to correct missed annotations, duplicate annotations, and inaccurate bounding boxes. The annotated dataset was randomly divided into training, validation, and test sets at a ratio of 8:1:1 as follows:

Training set: 555 images

Validation set: 69 images

Test set: 69 images

The dataset partitioning follows the general practice of deep learning experiments, ensuring that the training, validation, and test sets are mutually independent.

2.4. Methods

2.4.1. Improved YOLOv8 Detection Model

Basic Architecture

YOLOv8 consists of four main components: Input, Backbone, Neck, and Head [16–20]. In this study, the YOLOv8n model was systematically improved from three aspects: attention mechanism, feature fusion, and detection head.

BiFPN-Based Weighted Bidirectional Feature Pyramid Network

To enhance multi-scale feature representation, the original PAFPN was replaced with BiFPN. Learnable weights were introduced to adaptively fuse features at different scales and strengthen the information flow between high-level semantic features and low-level detailed features [21,22]. The structure of BiFPN is illustrated in Figure 2.

$$P_i^{td} = \frac{\omega_i^1 \times P_i + \omega_i^2 \times \mathrm{Upsample}\left(P_{i+1}^{td}\right)}{\omega_i^1 + \omega_i^2 + \varepsilon}, \tag{2}$$

In this equation, P_i^{td} represents the feature map obtained after fusion in the top-down pathway. ω_i^1 and ω_i^2 denote the learnable weight coefficients, while $\mathrm{Upsample}$ refers to the upsampling operation. ε is a small constant introduced to prevent division by zero.

$$P_i^{bu} = \frac{\omega_i^3 \times P_i^{td} + \omega_i^4 \times \mathrm{Downsample}\left(P_{i-1}^{bu}\right)}{\omega_i^3 + \omega_i^4 + \varepsilon}, \tag{3}$$

In this equation, P_i^{bu} denotes the fused feature representation generated through the bottom-up pathway. ω_i^3 and ω_i^4 are learnable weighting coefficients, and $\mathrm{Downsample}$ represents the downsampling operation.

$$P_i^{cs} = \frac{\omega_i^5 \times P_i^{bu} + \omega_i^6 \times \mathrm{CrossScale}\left(P_{i+k}^{cs}\right)}{\omega_i^5 + \omega_i^6 + \varepsilon}, \tag{4}$$

In this equation, P_i^{cs} denotes the feature map after cross-scale fusion. ω_i^5 and ω_i^6 are learnable weighting coefficients, and $\mathrm{CrossScale}$ represents the cross-scale operation, which can be either upsampling or downsampling. k indicates the offset relative to the current feature level.

GAM

To enhance feature representation, the Global Attention Mechanism (GAM) was incorporated. By integrating the channel attention module and the spatial attention module, the GAM strengthens feature information modeling, reduces information loss, and improves the model's representation capability for key target regions and important semantic features [23–25]. The structure of the GAM is illustrated in Figure 3.

$$z = [z_1, z_2, \ldots, z_c], \tag{5}$$

$$z_c = \frac{1}{H \times W} \times \sum_{i=1}^{H} \sum_{j=1}^{W} F_{i,j,c}, \tag{6}$$

$$F_{CA} = F \odot \sigma\big(W_2 \times \mathrm{ReLU}(W_1 \times z)\big), \tag{7}$$

In this equation, F denotes the input feature map with a size of $H \times W \times C$, and z_c is the average value of channel c. $F_{i,j,c}$ represents the value of the input feature map at position (i, j) in channel c. W_1 and W_2 are the weight matrices of the fully connected layers, σ denotes the activation function, F_{CA} represents the feature map weighted by channel attention, and $\odot$ denotes element-wise multiplication.

$$M_{SA} = \sigma\big(\mathrm{Conv}([\mathrm{AvP}(F); \mathrm{MaP}(F)])\big), \tag{8}$$

In this equation, $\mathrm{AvP}(F)$ denotes the average value at each spatial position, $\mathrm{MaP}(F)$ denotes the maximum value at each spatial position, M_{SA} represents the spatial attention weight map, and Conv denotes the convolution operation.

$$F_{GAM} = F_{CA} \odot M_{SA}, \tag{9}$$

In this equation, F_{GAM} denotes the final feature map weighted by global attention.

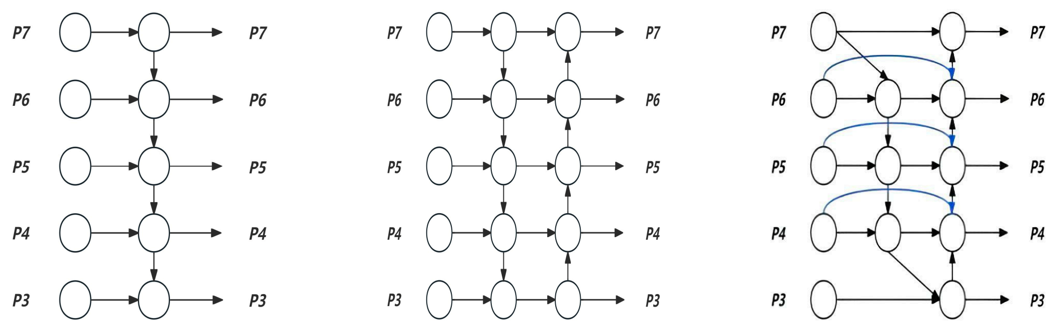

(**a**) (**b**) (**c**)

Figure 2. Structure comparison diagram. (**a**) FPN structure diagram; (**b**) PAFPN structure diagram. (**c**) BiFPN structure diagram.

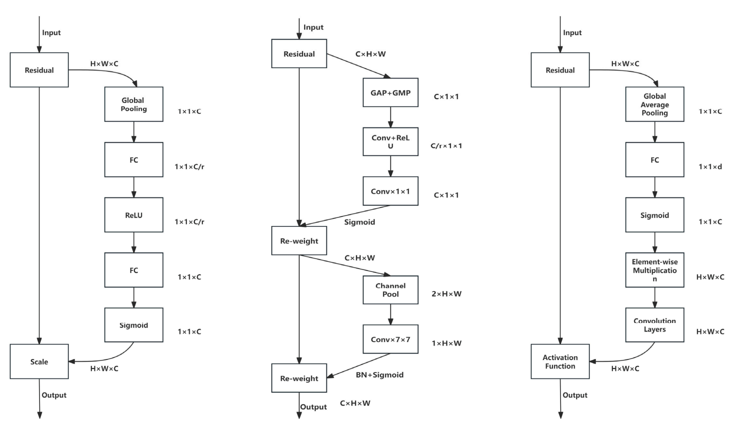

(**a**) (**b**) (**c**)

Figure 3. Comparison Diagram of Various Structures. (**a**) SE Structure Diagram; (**b**) CBAM Structure Diagram. (**c**) GAM Structure Diagram.

Small-Object Detection Layer

After feature fusion, the detection layer of the YOLOv8 model outputs feature maps at three different scales, namely 80 × 80, 40 × 40, and 20 × 20. These feature maps have different receptive fields and feature representations, making them suitable for detecting targets of different sizes. Specifically, high-resolution feature maps, such as 80 × 80 feature maps, have smaller receptive fields and can retain richer target location information and local detail features. Therefore, they are more beneficial for small-object detection. With feature maps at this scale, the model can locate small-sized targets in images more accurately, thereby reducing the risk of missed detection of small objects in complex scenarios to a certain extent.

In contrast, lower-resolution feature maps, such as 40 × 40 and 20 × 20 feature maps, have larger receptive fields and can extract richer global semantic information. These feature maps are generally used for detecting large objects, as they integrate more semantic information over a broader spatial range, but their ability to capture local details is relatively weakened. Owing to the different characteristics of these two types of feature maps, YOLOv8 can achieve strong performance in detecting objects of various sizes. However, to further improve the accuracy of small-object detection and reduce missed detections, this study structurally improved the original YOLOv8 model.

A high-resolution 160 × 160 detection layer was added to compensate for the insufficient resolution of the original 80 × 80 detection layer, thereby enhancing the localization and recognition of small and weak seedlings. This improvement is particularly effective for densely distributed and tiny maize seedlings.

Improved YOLOv8 Network Architecture

Several improvements were made to the YOLOv8 model to enhance its detection accuracy and robustness in maize seedling detection. In the improved YOLOv8 framework, the GAM was embedded into the Backbone network, BiFPN was adopted in the Neck part to replace the original PAFPN module, a 160 × 160 small-object detection head was added to the Head part, and the optimal detection boxes were finally output. The improved YOLOv8 network architecture is shown in Figure 4. Overall, the improved model achieves higher detection accuracy and better robustness in maize seedling detection, providing more reliable technical support for maize sowing quality evaluation and precise field seedling identification.

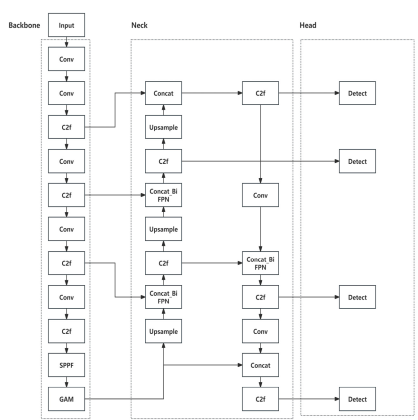

Figure 4. Structure diagram of improved model.

2.4.2. Maize Seedling Spacing Calculation

Maize Seedling Position Extraction

The images were recognized using the improved YOLOv8 model, through which the coordinates and confidence score of each detection box were obtained. The detection results included the coordinates of the upper-left and lower-right corners of the detection box, the target class label, and the detection confidence. Based on the detection box information, the center coordinates of each detection box were calculated and used as the position of the maize seedling. The center coordinates were calculated as follows:

$$x_c = \frac{x_{min}+x_{max}}{2},\ y_c = \frac{y_{min}+y_{max}}{2}, \tag{10}$$

In this equation, x_c denotes the horizontal coordinate of the center point, y_c denotes the vertical coordinate of the center point, x_{min} denotes the horizontal coordinate of the upper-left corner of the detection box, x_{max} denotes the horizontal coordinate of the lower-right corner of the detection box, y_{min} denotes the vertical coordinate of the upper-left corner of the detection box, and y_{max} denotes the vertical coordinate of the lower-right corner of the detection box.

When calculating plant spacing, pixel coordinates are usually used first and then further converted into actual distances, thereby establishing the correspondence between image space and real physical space. Since the output of the YOLOv8 model consists of normalized center coordinates, these coordinates need to be converted into pixel coordinates. The conversion formulas are as follows:

$$x_p = x_c \times image_w,\ y_p = y_c \times image_h, \tag{11}$$

where ypixel, x_p denotes the horizontal pixel coordinate, y_p denotes the vertical pixel coordinate, $image_w$ denotes the pixel width of the image, and $image_h$ denotes the pixel height of the image.

Row–Column Sorting

Row–column sorting is a key step in plant spacing calculation, as it can prevent crops in different rows or columns from being incorrectly identified as adjacent plants. First, column division is performed according to the horizontal coordinates of the seedling center points, and seedlings within the same column range are grouped together. Then, the seedlings in each column are sorted from top to bottom according to their vertical coordinates, providing positional information for subsequent plant spacing calculation.

$$C_k = \{P_i \mid |x_i - \overline{x}_k| \le T_x\}, \tag{12}$$

$$C_k^s = \mathrm{Sort}(C_k, y_i), \tag{13}$$

In this equation, P_i represents the center-point coordinates of maize seedling by i, C_k represents the seedling set in column k, $\overline{x}_k$ denotes the horizontal center coordinate of column k, T_x denotes the column division threshold, and C_k^s represents the seedling set in column k after being sorted in ascending order according to the vertical coordinates.

Average Plant Spacing Calculation

- Linear Average Plant Spacing Calculation

For the calculation of plant spacing among maize seedlings located in the same column, only the vertical distance needs to be considered. The formula is as follows:

$$Dis_i = |y_{p,i} - y_{p,i-1}|, \tag{14}$$

where ypixel, $y_{p,i}$ denotes the vertical pixel coordinate of the seedling indexed by i, and Dis_i represents the pixel distance between the seedling indexed by (i) and the previous seedling.

Since plant spacing was first calculated in the image coordinate system, the obtained spacing values were expressed in pixels and needed to be converted into actual physical distances. In this study, the actual length and width of the photographed field area were measured in the field and used as spatial calibration references. Based on the image resolution and the corresponding real field size, the physical distance represented by each pixel was calculated. The pixel spacing between adjacent maize seedlings was then multiplied by the conversion factor to obtain the actual plant spacing in centimeters. The conversion formula is as follows:

$$\mathrm{Conversion\_Fa_x} = \frac{\mathrm{actual_l}}{\mathrm{image_w}}, \tag{15}$$

$$\mathrm{Conversion\_Fa_y} = \frac{\mathrm{actual_w}}{\mathrm{image_h}}, \tag{16}$$

$$\mathrm{Average\_Sp_s} = \frac{1}{n} \times \sum_{i=1}^{n} \left(\mathrm{Dis_i} \times \frac{\mathrm{Conversion\_Fa_x} + \mathrm{Conversion\_Fa_y}}{2} \right), \tag{17}$$

In this equation, $\mathrm{actual_l}$ denotes the actual length of the photographed area, $\mathrm{actual_w}$ denotes the actual width of the photographed area, $\mathrm{Conversion\_Fa_x}$ denotes the actual length corresponding to each pixel, $\mathrm{Conversion\_Fa_y}$ denotes the actual width corresponding to each pixel, n denotes the number of adjacent seedling pairs in the same column, and $\mathrm{Average\_Sp_s}$ denotes the average plant spacing.

- Plant Spacing Calculation on Curved Rows

Plant spacing calculation on curved rows is more complex than that on straight rows, because factors such as curvature, radius, and central angle need to be considered. On a curved row, maize seedlings are usually distributed along an arc. Therefore, the basic parameters of the arc need to be fitted, including the radius of the curved row and the position of the circle center. The circle center and radius of the arc can be estimated from the known positions of multiple seedlings. The formulas are as follows:

$$(x_{c,i} - x_0)^2 + (y_{c,i} - y_0)^2 = R^2, \tag{18}$$

In this equation, x_0 and y_0 represent the horizontal and vertical coordinates of the fitted circle center, respectively, and R represents the fitted radius. This equation indicates that the distance from each seedling position to the circle center is equal to the radius. By fitting multiple points using the least squares method, the circle center and radius of the curved row can be estimated. The fitting process is essentially to find an optimal circle so that all seedling positions are as close as possible to the corresponding arc.

The curvature of the curved row can be represented by an angle, which determines the arc length and curvature of the row. To estimate this angle, the starting point and ending point of the curved row need to be considered. A larger angle indicates a higher degree of curvature. The formula is given as follows:

$$\theta = \arctan\left(\frac{y_{c,n} - y_0}{x_{c,n} - x_0}\right) - \arctan\left(\frac{y_{c,1} - y_0}{x_{c,1} - x_0}\right), \tag{19}$$

In this equation, θ represents the central angle, $x_{c,1}$ and $y_{c,1}$ represent the coordinates of the starting point of the curved row, and $x_{c,n}$ and $y_{c,n}$ represent the coordinates of the ending point of the curved row. In a curved row, the spacing between adjacent seedlings cannot be measured simply by the straight-line distance. To calculate the arc length between each pair of adjacent seedlings, the angular difference between these seedlings along the curved row needs to be calculated. Based on this, the average plant spacing of maize seedlings in the curved row can be obtained. The formula is given as follows:

$$\Delta\theta_i = \frac{\theta}{n-1}, \tag{20}$$

$$\mathrm{Ground_i} = R \times \Delta\theta_i, \tag{21}$$

$$\text{Average\_Sp}_c = \frac{R \times \theta}{n - 1}, \quad (22)$$

where ypixel, $\Delta\theta_i$ represents the angular difference in radians between two adjacent seedlings, Ground_i denotes the actual physical distance between the seedlings, and Average_Sp_c denotes the average plant spacing in the curved row.

Evaluation Indicators of Sowing Quality

In this study, the average plant spacing and its deviation relative to the target plant spacing were used as evaluation criteria to assess the sowing quality of the seeder.

$$\text{Average\_Sp}_t = \frac{L_s \times \text{Average\_Sp}_s + s \times \text{Average\_Sp}_c}{L_s + s}, \quad (23)$$

$$\delta = \left| \frac{\text{Average\_Sp}_t - \text{Average\_Sp}_g}{\text{Average\_Sp}_g} \right| \times 100\%, \quad (24)$$

where ypixel, Average_Sp_t represents the overall average plant spacing; L_s represents the total length of the straight segments; Average_Sp_g represents the target average plant spacing, namely 32 cm; and δ represents the deviation of the average plant spacing. A value of $\delta \leq 5\%$ indicates high-quality sowing.

3. Results

3.1. Experimental Environment

The experimental environment was established on an AutoDL workstation, and the main configurations are as follows:

- Hardware: Intel Xeon Platinum 8358P, RTX 3090 (24 GB)
- System: Ubuntu 20.04, CUDA 11.8, PyTorch 2.0.0
- Parameters: input size of 640 × 640, batch = 16, epoch = 800, lr = 0.01

3.2. Evaluation Metrics

In this study, Precision, Recall, mAP50, and mAP50–95 were mainly used as evaluation metrics to assess the performance of the improved model.

The related calculation formulas are as follows:

$$\text{Recall} = \frac{TP}{TP + FN}, \quad (25)$$

$$\text{Precision} = \frac{TP}{TP + FP}, \quad (26)$$

$$\text{mAP} = \frac{\sum_{i=1}^{k} AP_i}{k}, \quad (27)$$

In this equation, TP denotes true positives, indicating that positive samples are correctly identified as positive samples. FN denotes false negatives, indicating that positive samples are incorrectly identified as negative samples. FP denotes false positives, indicating that negative samples are incorrectly identified as positive samples. AP_i refers to the average precision of the detection class indexed by i, namely the area under the PR curve. mAP is obtained by summing the average precision values and dividing them by the number of classes, representing the mean average precision.

3.3. Model Performance Analysis

3.3.1. Ablation Experiment

To verify the effects of each improved module on the recognition accuracy of YOLOv8, ablation experiments were conducted for comparison. The results are shown in Table 1.

Table 1. Results of ablation experiment.

Model				P	R	mAP50	mAP50-95
	BiFPN	GAM	Small-target-detection-layer				
YOLOv8n	×	×	×	86.8	89.8	92.9	46.7
	√	×	×	87.8	90.1	93.1	48.4
	×	√	×	88.3	89.7	93.2	48.7
	×	×	√	88.7	89.7	93.8	48.5
	√	√	√	89.4	90.3	94.4	49.4

Note: "√" indicates that the corresponding module is used, while "×" indicates that the corresponding module is not used.

Table 1 presents the ablation experiment results of the improved YOLOv8 model under different module combinations. By progressively introducing BiFPN, the GAM, and the small-object detection layer, the experiment analyzes the influence of each module on the detection performance of the model.

First, the original YOLOv8n model was used as the baseline model. Without introducing BiFPN, the GAM attention module, or the small-object detection layer, the model achieved a precision of 86.8%, a recall of 89.8%, an mAP50 of 92.9%, and an mAP50-95 of 46.7%. These results provide a baseline reference for evaluating the effectiveness of the subsequent improvements.

When BiFPN was introduced alone, the model achieved a precision of 87.8%, a recall of 90.1%, an mAP50 of 93.1%, and an mAP50–95 of 48.4%, indicating that BiFPN improved multi-scale feature fusion. With only the GAM, the precision increased to 88.3%, while the recall slightly decreased to 89.7%; meanwhile, mAP50 and mAP50–95 reached 93.2% and 48.7%, respectively, showing that the GAM enhanced key feature representation. When only the small-object detection layer was added, the precision increased to 88.7%, the recall remained at 89.7%, and mAP50 and mAP50–95 reached 93.8% and 48.5%, respectively, demonstrating its effectiveness in improving the localization and recognition of small maize seedlings.

Finally, the complete improved model, which simultaneously incorporated BiFPN, the GAM, and the small-object detection layer, achieved the best overall performance. The model obtained a precision of 89.4%, a recall of 90.3%, an mAP50 of 94.4%, and an mAP50-95 of 49.4%. These results indicate that the detection performance of the model was further improved. The three improved modules show a certain degree of complementarity, as they jointly enhance the multi-scale feature fusion capability, key feature representation capability, and small-object detection capability of the model, thereby improving the accuracy and robustness of maize seedling detection.

In summary, the ablation experiment results demonstrate that the introduction of BiFPN, the GAM, and the small-object detection layer all had positive effects on the detection performance of the YOLOv8n model. After the three modules were combined, the model achieved the best results in terms of precision, recall, mAP50, and mAP50-95, indicating that the improved strategy proposed in this study can effectively enhance maize seedling detection performance. The detection results of the improved YOLOv8 model are shown in Figure 5.

Figure 5. Identification result diagram.

3.3.2. Comparative Experiment

To verify the performance of the improved YOLOv8 model in maize seedling recognition, comparative experiments were conducted between the improved model and several mainstream neural network models. YOLOv5, YOLOv6, YOLOv8, YOLOv8-p2, YOLOv10 and Faster R-CNN were selected for comparison. All models were trained and tested using the same dataset and the experimental parameters described above. The final experimental results are shown in Table 2.

Table 2. Comparison test results of seedling identification.

Model	P	R	mAP50	mAP50-95
Improved model	89.4	90.3	94.4	49.4
YOLOv5	88.2	88.2	92	45.8
YOLOv6	85.9	85.7	90.3	44.3
YOLOv8	86.8	89.8	92.9	46.7
YOLOv8-p2	88.6	89.6	93.7	48.6
YOLOv10	88.5	90.1	93.5	48.8
Faster R-CNN	88.9	90.5	93.8	47.6

As shown in Table 2, compared with current mainstream object detection models, the improved YOLOv8 model proposed in this study achieved superior performance under the same experimental conditions. Specifically, the improved YOLOv8 model reached a precision of 89.4% and a recall of 90.3%. In addition, its mean average precision, mAP50, reached 94.4%, outperforming the other models.

To further verify the practical performance of the improved YOLOv8 model in plant spacing measurement, a comparative experiment with the original model was conducted. Taking the maize seedlings detected in Figure 6 as an example, the image contained a total of 50 seedlings. The center-point coordinates of the seedlings were extracted using the two models, and the recognition results are presented in Appendix Table A1.

As shown in Table A1, the original YOLOv8 model extracted the center points of 34 maize seedlings, while the improved model increased this number to 48. The coordinate positions obtained by the two models showed no obvious differences. However, in regions where seedlings were closely spaced and densely distributed, the improved model achieved more accurate recognition and effectively reduced missed and false detections. In particular, for dense target extraction, the improved model demonstrated stronger discrimination capability, enabling it to clearly distinguish adjacent seedlings and improve the overall completeness of recognition.

https://doi.org/10.3390/agriculture16161746

Figure 6. Example of maize Seedlings.

3.4. Sowing Quality Evaluation

Sowing Quality Evaluation and Result Verification

After processing the maize seedling images, the target recognition results extracted by the YOLOv8 model were combined with coordinate restoration and distance measurement methods to quantitatively analyze the spacing between adjacent seedlings. The final average plant spacing between adjacent seedlings was 30.42 cm, and the deviation relative to the target plant spacing was 4.93%. The overall deviation was relatively small, indicating that the sowing density was reasonably controlled and that the overall sowing quality was high.

To further verify the reliability of the results and analyze their consistency across different data sources, a multidimensional comparative analysis was conducted using the sample plot shown in Figure 6 as an example. The analysis combined the target plant spacing, field-measured data, and the recognition results obtained by the YOLOv8 model. A total of 57 sowing positions were set in the plot, among which 50 seedlings emerged and 7 seedlings were missing. Among the missing seedlings, 2 were caused by missed sowing by the seeder, while 5 failed to emerge due to abnormal seed development. The seeder was set to a target plant spacing of 32 cm. The field-measured average plant spacing was 33.56 cm, with a deviation of 4.87% relative to the target spacing. The average plant spacing calculated based on YOLOv8 recognition was 34.76 cm, with a deviation of 3.57% relative to the field-measured spacing.

For plant spacing distribution analysis, the spacing between adjacent seedlings was further measured, and the results are shown in Appendix Table A2. To validate the accuracy of plant spacing estimation against field measurements, the field-measured plant spacing was used as the reference value, while the plant spacing calculated by the original YOLOv8 model and the improved model was used as the estimated value. Several statistical error metrics were calculated, including mean absolute error (MAE), root mean square error (RMSE), mean relative error (MRE), and mean bias error (MBE). The results are shown in Table 3.

Table 3. Statistical error comparison of plant spacing estimation between the original YOLOv8 model and the improved model.

Model	MAE (m)	RMSE (m)	MRE (%)	MBE (m)
Original YOLOv8	0.1416	0.2357	43.14	0.0416
Improved YOLOv8	0.0317	0.0683	10.34	0.109

As shown in Table 3, the improved model achieved lower plant spacing estimation errors than the original YOLOv8 model. Specifically, the MAE, RMSE, and MRE decreased from 0.1416 m, 0.2357 m, and 43.14% to 0.0317 m, 0.0683 m, and 10.34%, respectively. The MBE also decreased from 0.0416 m to 0.0109 m, indicating that the improved model reduced the overall bias in plant spacing estimation. In addition, as shown in Figure 7, most scatter points of the improved model were distributed near the 1:1 reference line, further indicating good consistency between the calculated and field-measured plant spacing. Although relatively large errors still occurred in some abnormal spacing regions, the improved model provided more accurate and reliable plant spacing estimation under the tested field conditions.

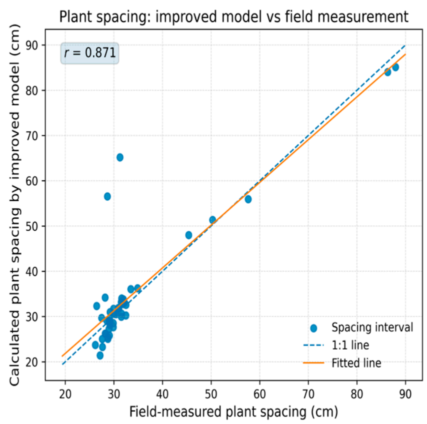

Figure 7. Relationship between field-measured plant spacing and plant spacing calculated by the improved model.

In addition, for missing seedling identification, five obvious abnormal spacing regions were recorded in the field measurements, including three regions exceeding 45 cm and two regions greater than 80 cm, corresponding to seven non-emerged seeds. The image recognition results also detected spacing abnormalities at the same positions, showing high consistency with the field-measured data. This indicates that the proposed method can not only accurately identify normal seedlings but also effectively capture problems such as missed sowing and abnormal seed development.

In summary, the YOLOv8-based image recognition method showed stable performance in plant spacing measurement and missing seedling identification. It can be used to quantify sowing performance, evaluate sowing consistency, and assess seed development, providing reliable technical support for precision sowing management and intelligent agricultural production.

4. Discussion

Compared with previous studies on maize seedling detection, plant counting, and crop population measurement, and seedling quality assessment, the proposed method places more emphasis on the transformation from seedling detection to quantitative plant spacing measurement and sowing quality evaluation. Ren et al. combined YOLOv8 object detection with Voronoi spatial analysis to evaluate maize seedling quality from UAV images [26]. Their study mainly focused on seedling quality assessment and spatial distribution analysis, whereas the present study further calculates the spacing between adjacent seedlings through center-point extraction and row–column sorting and validates the plant spacing estimation results using field-measured data. Gao et al. proposed a Maize-YOLOv8n-based method for detecting maize seedling leakage from UAV images and combined image processing, row fitting, and average plant distance calculation to identify missing seedlings [27]. Compared with their work, this study not only detects missing seedlings but also evaluates plant spacing estimation accuracy using the MAE, RMSE, MRE, MBE, and Pearson correlation coefficient. Jia et al. compared different deep learning models for maize seedling number detection using UAV images and analyzed the effects of growth stage, planting density, and flight altitude on detection performance [28]. In contrast, this study focuses not only on seedling recognition performance but also on the subsequent use of detection results for plant spacing measurement and sowing quality assessment. Wu et al. developed an H-RT-DETR-based method for maize seedling recognition in UAV remote sensing images [29]. Their study mainly improved seedling recognition accuracy, while the proposed method further links object detection results with agronomic spacing indicators. Wang et al. proposed a Maize-YOLO-based method for maize seedling detection and missing seedling rate estimation from UAV imagery [30]. Different from missing seedling rate estimation, this study provides interval-level plant spacing estimation and compares the estimated spacing with field measurements.

Overall, existing studies have made important progress in maize seedling detection, counting, missing seedling identification, and seedling quality assessment. However, most of them mainly focus on detection accuracy, plant number extraction, or missing seedling recognition. In contrast, the proposed method integrates image preprocessing, maize seedling detection, center-point extraction, row–column sorting, plant spacing calculation, field-measured validation, and sowing quality evaluation into a unified workflow. Therefore, this study not only identifies maize seedlings but also provides quantitative support for plant spacing measurement, missing seedling monitoring, and seeder parameter optimization under the tested field conditions.

Although the proposed method was evaluated using images collected from the experimental field, the detailed plant spacing analysis presented in Figure 6 was based on a representative sample of 50 emerged maize seedlings. Therefore, this sample-based analysis should be interpreted as a case demonstration of the proposed workflow rather than as the only validation of the method. Beyond this sample-level validation, the generalizability of the proposed method may also be affected by the limited number of acquisition locations, dates, and environmental conditions, because these factors can lead to differences in image distribution and field characteristics. First, images collected from a single experimental field may not fully represent variations in soil color, ridge–furrow structure, straw residue coverage, sowing patterns, and field management conditions in other regions. Second, images collected during a limited acquisition period may not cover changes in seedling size, leaf morphology, canopy structure, and weed interference at different growth stages. Third, limited environmental conditions may not fully reflect variations in illumination, shadows, haze, sand–dust intensity, image contrast, and spatial resolution. These differences may affect seedling detection confidence, center-point localization accuracy, row–column sorting, and the subsequent conversion from pixel spacing to physical plant spacing. Therefore, although the proposed method showed good performance under the tested field conditions, further validation using multi-location, multi-date, multi-growth-stage, and multi-environment datasets is still needed to evaluate and improve its robustness and generalizability.

5. Conclusions

This study proposes an improved YOLOv8-based method for maize seedling detection and intelligent plant spacing measurement. Through the collaborative optimization of the GAM, BiFPN feature fusion, and a small-object detection layer, the proposed method improves seedling recognition accuracy and the reliability of plant spacing measurement under complex field conditions. The experimental results show that the improved model achieved an mAP50 of 94.4%, while the relative error of plant spacing measurement compared with the preset sowing spacing was 4.93%. These results indicate that the proposed method can provide technical support for sowing quality evaluation, missing seedling monitoring, and seeder parameter optimization under the tested field conditions. In future work, multi-stage time-series data will be further integrated to construct a dynamic monitoring system covering the whole growth period, thereby supporting digital and precise management of large-scale farmland.

Author Contributions: P.Z.: Formal analysis, Methodology, Project administration, Software, Writing—original draft; S.Y.: Data curation, Investigation, Validation; G.T.: Conceptualization, Writing—review & editing. All authors have read and agreed to the published version of the manuscript.

Funding: This research was funded by the National Natural Science Foundation of China (grant number U20A20180).

Institutional Review Board Statement: Not applicable.

Data Availability Statement: The original contributions presented in this study are included in the article. Further inquiries can be directed to the corresponding author.

Acknowledgments: We appreciate the technical support provided by the team we are a part of.

Conflicts of Interest: The authors declare no conflicts of interest.

Appendix A

Table A1. Extraction Results of Center Point Coordinates.

YOLOv8		Improved Model	
Center-x	**Center-y**	**Center-x**	**Center-y**
2273.5749	952.7386	2433.036	1022.85
3178.4025	1914.3235	3069.392	1966.101
2463.5804	2014.7048	2365.34	1849.143
2920.7468	2375.5866	2975.756	2385.459
152.3773	1918.4803	182.5236	1813.926
1875.8623	1188.4649	365.9612	685.197
3030.0059	892.5434	1734.048	1012.587
3822.9601	2202.3463	3083.412	791.823
156.0433	917.1566	985.46	1208.823
1728.2125	1342.0498	945.604	1585.476
1926.9008	697.3361	3835.216	2088.426
3747.9229	173.1680	291.1944	1052.904
1763.9172	424.2214	1648.496	1331.757
2692.5996	273.6392	1743.264	576.696
824.7443	2345.6217	3823.82	167.151
1055.0820	505.3217	1802.972	229.5069
3142.0810	1552.9229	2502.14	300.378
77.7467	2350.3684	802.068	2339.544
329.6219	2895.7846	1089.372	430.842
3197.7022	3045.8871	3070.668	1587.399
234.1361	1220.3491	100.6224	2180.196
798.2350	2044.8999	149.6544	2857.596
127.5058	1824.4054	2999.804	2870.766
1540.9884	2649.9603	207.6688	1402.809
1040.9729	62.3279	871.276	1940.907

1737.6714	1960.7729	126.8248	1652.925
3307.7417	418.6269	1509.316	2511.9
2404.8920	553.6656	721.392	2794.422
783.7949	2847.1510	3796.276	1766.097
604.1795	330.9617	1615.408	1682.007
1140.9780	871.5291	1127.196	159.0717
2981.4694	985.4139	1586.772	2002.044
3728.8738	2533.5572	3168.104	354.195
2858.2576	1205.6279	1026.872	872.67
----	----	3837.012	948.666
----	----	2446.324	596.811
----	----	711.264	2683.041
----	----	1131.784	95.3838
----	----	454.276	284.8173
----	----	901.612	1846.986
----	----	2293.36	2188.926
----	----	3788.556	1299.168
----	----	3177.788	418.428
----	----	3058.64	1131.057
----	----	1129.68	137.3076
----	----	3084.844	1124.715
----	----	709.332	2699.883
----	----	1059.284	848.862

Table A2. Analysis of plant spacing results.

YOLOv8 (m)	Improved Model (m)	Field Measurement (m)
0.2419	0.3320	0.3149
0.2467	0.2762	0.2987
0.4015	0.3398	0.3158
0.3480	0.3053	0.3044
0.2443	0.2853	0.2988
0.5523	0.5592	0.5763
0.2654	0.3279	0.3167
0.2545	0.3176	0.3102
0.7776	0.3311	0.3215
0.2318	0.8513	0.8795
0.8577	0.3231	0.2645
0.2685	0.3172	0.2992
0.2169	0.3022	0.3245
0.3022	0.3060	0.3012
0.2154	0.2622	0.2817
0.7972	0.6518	0.3124
0.2686	0.3257	0.3248
0.2853	0.3191	0.3095
0.2798	0.2881	0.2911
0.3202	0.3065	0.2988
0.2741	0.2916	0.2918
0.2505	0.2994	0.3152
0.6645	0.3065	0.3156
0.3902	0.2580	0.2907
0.2143	0.3098	0.2919
0.2208	0.2813	0.2916

0.8658	0.2910	0.2897
0.5801	0.2846	0.2944
0.2784	0.2540	0.2879
0.2180	0.2968	0.2745
0.2652	0.2614	0.2831
0.2976	0.2139	0.2714
0.2013	0.3419	0.2819
----	0.2722	0.2894
----	0.3381	0.3194
----	0.3603	0.3346
----	0.2507	0.2875
----	0.3623	0.3485
----	0.2325	0.2764
----	0.2907	0.2853
----	0.2371	0.2617
----	0.2503	0.2759
----	0.5133	0.5031
----	0.8404	0.8632
----	0.4799	0.4538
----	0.5654	0.2866
----	0.3289	0.3187
----	----	0.2876
----	----	0.3285

References

1. Liu, M.; Su, W.-H.; Wang, X.-Q. Quantitative evaluation of maize emergence using UAV imagery and deep learning. *Remote Sens.* **2023**, *15*, 1979.
2. Zhang, H.; Fu, Z.; Han, W.; Yang, G.; Niu, D.; Zhou, X. Detection method of maize seedlings number based on improved YOLO. *Trans. Chin. Soc. Agric. Mach.* **2021**, *52*, 221–229.
3. Petrović, I.; Vučajnk, F.; Trdan, S.; Bernik, R.; Vidrih, M. The Influence of Planting Speed of a Maize Vacuum Planter on Plant Spacing Variability and Ear Parameters. *Agronomy* **2025**, *15*, 462.
4. Zhu, H.; Lin, C.; Liu, G.; Wang, D.; Qin, S.; Li, A.; Xu, J.-L.; He, Y. Intelligent agriculture: Deep learning in UAV-based remote sensing imagery for crop diseases and pests detection. *Front. Plant Sci.* **2024**, *15*, 1435016.
5. Shrestha, D.S.; Steward, B.L. Automatic corn plant population measurement using machine vision. *Trans. ASAE* **2003**, *46*, 559.
6. Shi, Y.; Wang, N.; Taylor, R.; Raun, W. Improvement of a ground-LiDAR-based corn plant population and spacing measurement system. *Comput. Electron. Agric.* **2015**, *112*, 92–101.
7. Jia, H.; Wang, G.; Guo, M.; Dylan, S.; Jiang, X.; Zhao, J. Methods and experiments of obtaining corn population based on machine vision. *Trans. Chin. Soc. Agric. Eng.* **2015**, *31*, 215–220.
8. Tian, Z.; Fu, Y.; Liu, S. Rapid crops classification based on UAV low-altitude remote sensing. *Trans. Chin. Soc. Agric. Eng.* **2013**, *29*, 109–116.
9. Wenli, J.; Zhou, L.; Haihua, X. Lightweight Method for Identifying Farmland Weeds Based on YOLO v5. *Nongye Jixie Xuebao/Trans. Chin. Soc. Agric. Mach.* **2024**, *55*, 212–222+293.
10. Wang, F.; Wang, Q.; Chen, J.; Liu, F. Improved faster r-cnn target detection algorithm based on attention mechanism and soft-nms. *Laser Optoelectron. Progress* **2021**, *58*, 2420001.
11. Meng, Q.; Zhang, M.; Yang, X.; Liu, Y.; Zhang, Z. Recognition of maize seedling and weed based on light weight convolution and feature fusion. *Trans. Chin. Soc. Agric. Mach.* **2020**, *51*, 238–245.
12. Gnädinger, F.; Schmidhalter, U. Digital counts of maize plants by unmanned aerial vehicles (UAVs). *Remote Sens.* **2017**, *9*, 544.
13. Liu, S.; Yang, G.; Zhou, C.; Jing, H.; Feng, H.; Xu, B.; Yang, H. Extraction of maize seedling number information based on UAV imagery. *Trans. Chin. Soc. Agric. Eng.* **2018**, *34*, 69–77.
14. Lu, C.; Nnadozie, E.; Camenzind, M.P.; Hu, Y.; Yu, K. Maize plant detection using UAV-based RGB imaging and YOLOv5. *Front. Plant Sci.* **2024**, *14*, 1274813.

15. Li, B.; Peng, X.; Wang, Z.; Xu, J.; Feng, D. Aod-net: All-in-one dehazing network. In *Proceedings of the 2017 IEEE International Conference on Computer Vision (ICCV)*; IEEE: Piscataway, NJ, USA, 2017; pp. 4780–4788.
16. Redmon, J.; Divvala, S.; Girshick, R.; Farhadi, A. You only look once: Unified, real-time object detection. In *Proceedings of the IEEE Conference on Computer Vision and Pattern Recognition*; IEEE: Piscataway, NJ, USA, 2016; pp. 779–788.
17. Redmon, J.; Farhadi, A. YOLO9000: Better, faster, stronger. In *Proceedings of the IEEE Conference on Computer Vision and Pattern Recognition*; IEEE: Piscataway, NJ, USA, 2017; pp. 7263–7271.
18. Redmon, J.; Farhadi, A. Yolov3: An incremental improvement. *arXiv* **2018**, arXiv:1804.02767.
19. Bochkovskiy, A.; Wang, C.-Y.; Liao, H.-Y.M. Yolov4: Optimal speed and accuracy of object detection. *arXiv* **2020**, arXiv:2004.10934.
20. Terven, J.; Córdova-Esparza, D.-M.; Romero-González, J.-A. A comprehensive review of yolo architectures in computer vision: From yolov1 to yolov8 and yolo-nas. *Mach. Learn. Knowl. Extr.* **2023**, *5*, 1680–1716.
21. Lin, T.-Y.; Dollár, P.; Girshick, R.; He, K.; Hariharan, B.; Belongie, S. Feature pyramid networks for object detection. In *Proceedings of the IEEE Conference on Computer Vision and Pattern Recognition*; IEEE: Piscataway, NJ, USA, 2017; pp. 2117–2125.
22. Tan, M.; Pang, R.; Le, Q.V. Efficientdet: Scalable and efficient object detection. In *Proceedings of the IEEE/CVF Conference on Computer Vision and Pattern Recognition*; IEEE: Piscataway, NJ, USA, 2020; pp. 10781–10790.
23. Hu, J.; Shen, L.; Sun, G. Squeeze-and-excitation networks. In *Proceedings of the IEEE Conference on Computer Vision and Pattern Recognition*; IEEE: Piscataway, NJ, USA, 2018; pp. 7132–7141.
24. Li, L.; Shibo, L.; Hao, R.; Gang, X.; Yongzhong, Z. Mulberry branch identification and location method based on improved YOLO v5 in complex environment. *Nongye Jixie Xuebao/Trans. Chin. Soc. Agric. Mach.* **2024**, *55*, 249–257.
25. Liu, Y.; Shao, Z.; Hoffmann, N. Global attention mechanism: Retain information to enhance channel-spatial interactions. *arXiv* **2021**, arXiv:2112.05561.
26. Ren, L.; Li, C.; Yang, G.; Zhao, D.; Zhang, C.; Xu, B.; Feng, H.; Chen, Z.; Lin, Z.; Yang, H. The detection of maize seedling quality from UAV images based on deep learning and Voronoi diagram algorithms. *Remote Sens.* **2024**, *16*, 3548.
27. Gao, J.; Tan, F.; Cui, J.; Hou, Z. Unmanned aerial vehicle image detection of maize-YOLOv8n seedling leakage. *Front. Plant Sci.* **2025**, *16*, 1569229.
28. Jia, Z.; Zhang, X.; Yang, H.; Lu, Y.; Liu, J.; Yu, X.; Feng, D.; Gao, K.; Xue, J.; Ming, B. Comparison and optimal method of detecting the number of maize seedlings based on deep learning. *Drones* **2024**, *8*, 175.
29. Wu, Y.; Yuan, S.; Tang, L. Plant recognition of maize seedling stage in UAV remote sensing images based on H-RT-DETR. *Plant Methods* **2025**, *21*, 60.
30. Wang, L.; Zhang, Y.; Sun, Z.; Gao, Y.; Wang, Y. Detection and Estimation of Missing Maize Seedlings via UAV Imagery and Maize-YOLO. *Appl. Soft Comput.* **2026**, *197*, 115195.

https://doi.org/10.3390/agriculture16161746